IJRCS

International Journal of Robotics and Control Systems
Vol. 5, No. 6, 2025, pp. 3047-3063
ISSN 2775-2658
http://pubs2.ascee.org/index.php/ijrcs

ASCEE

Implementation of Fuzzy Kalman Filter in Indoor Localization Using Ultra-Wideband Sensor

Riky Dwi Puriyanto [a,1,*], Haris Imam Karim Fathurrahman [a,2], Faisal Fajri Rahani [b,3], Efa Wakhidatus Solikhah [c,3], Zalili Binti Musa [d,3]

[a] Department of Electrical Engineering, Universitas Ahmad Dahlan, Indonesia
[b] Department of Informatics, Universitas Ahmad Dahlan, Indonesia
[c] Department of Management, Universitas Ahmad Dahlan, Indonesia
[d] Faculty of Computing, Universiti Malaysia Pahang Al-Sultan Abdullah, Malaysia
[1] rikydp@ee.uad.ac.id; [2] haris.fathurrahman@te.uad.ac.id; [3] faisal.fajri@tif.uad.ac.id; [4] efa.solikhah@mgm.uad.ac.id;
[5] zalili@umpsa.edu.my
[*] Corresponding Author

ARTICLE INFO

Article History
Received June 26, 2025
Revised October 27, 2025
Accepted December 16, 2025

Keywords
Ultra-Wideband Sensor;
Kalman Filter;
Fuzzy Logic;
Trilateration;
Indoor Localization

ABSTRACT

Indoor localization is an essential technology for indoor position tracking, one of which utilizes Ultra-Wideband (UWB) sensors because of their high accuracy. However, UWB sensor readings still contain noise that reduces data reliability. To overcome this, this study proposes a solution in the form of a Kalman Filter with adaptive determination of process noise (Q) and measurement noise (R) values based on fuzzy logic. The main contribution of this study is the application of Fuzzy Kalman Filter (FKF) to dynamically adjust Q and R values, thereby increasing resistance to noise. The method used is the Mamdani fuzzy logic system integrated into the Kalman Filter, where fuzzy rules regulate Q and R updates based on variations in estimation errors. Performance analysis uses Root Mean Square Error (RMSE) and Mean Absolute Error (MAE). The experimental results show that applying the Fuzzy Kalman Filter to UWB sensor readings can significantly reduce RMSE and MAE values. Almost the same RMSE and MAE values indicate increased accuracy and outlier reduction. In addition, using the Kalman Filter affects the estimation of tag position coordinates obtained from the Trilateration method, thereby reducing deviation and producing more stable RMSE and MAE values. This study concludes that the Fuzzy Kalman Filter successfully improves the accuracy of UWB-based indoor localization while reducing noise and outliers in measurement data.

1. Introduction

Localization is a way to determine the location of an object in an environment. Localization-based services are needed in various areas of life [1]–[3]. The system requires accurate object position information to make correct decisions, both in indoor and outdoor environments. Indoor localization requires better accuracy because it generally covers a limited environment [4]. Indoor localization is implemented in various applications, such as automated cleaning robots [5]–[7], real-time luggage tracking at airports [8], [9], hospital equipment monitoring (such as wheelchairs and defibrillators) [10], [11], worker/item location tracking [12], and restricted access control for high-security zones

[13].

There are several methods used in indoor localization, including: Wi-Fi-based localization [14], [15], Bluetooth Low Energy (BLE) and Beacon [16], [17], Ultra-Wideband (UWB) [18], [19], computer vision and camera [20], [21], Inertial Measurement Unit (IMU) [22], [23], and LiDAR [24], [25]. Wi-Fi-based localization leverages Received Signal Strength Indicator (RSSI) measurements from multiple access points (APs) to estimate position through trilateration or fingerprinting techniques [26], [27]. BLE-based localization employs iBeacon or Eddystone transmitters that broadcast signals detected by mobile devices [28]. Distance estimation relies on RSSI, with proximity detection or trilateration used for positioning. BLE beacons are energy-efficient and cost effective, making them suitable for retail and indoor navigation applications. UWB provides centimeter-level accuracy by measuring the Time of Flight (ToF) or Time Difference of Arrival (TDoA) of ultrashort pulse signals between anchors and tags [29]. Its resistance to multipath interference and high temporal resolution make it ideal for industrial tracking and autonomous robotics.

Computer Vision and Camera-based systems use optical sensors and advanced algorithms to detect and track objects by analyzing visual data, enabling applications like augmented reality navigation and robotic perception. However, they are heavily dependent on lighting conditions [30]. Inertial Measurement Units (IMUs), consisting of accelerometers, gyroscopes, and magnetometers, estimate motion and orientation through dead reckoning, providing real-time tracking, but suffering from cumulative drift errors over time [31]. Light Detection and Ranging (LiDAR) employs laser pulses to generate precise 3D depth maps, offering centimeter-level accuracy for autonomous vehicles and 3D mapping, but at higher costs and computational demands [32]. These technologies are often fused (e.g. visual-inertial odometry or LiDAR-SLAM) to enhance robustness in indoor localization, autonomous systems, and augmented reality applications.

UWB technology offers significant advantages over other indoor localization methods, making it the preferred choice for high-precision applications. This approach makes UWB highly resistant to multipath interference and signal noise, problems that often degrade the performance of Wi-Fi and BLE in complex environments. Additionally, UWB operates with extremely low latency, enabling real-time tracking at refresh rates exceeding 100 Hz. This becomes a critical feature for dynamic applications such as autonomous robotics and industrial automation that other technologies cannot match [33]. Another key advantage is UWB's ability to penetrate obstacles while maintaining accuracy, unlike optical systems that fail when line-of-sight is obstructed. UWB technology uses efficient energy, which can be implemented on devices with battery power sources [34].

UWB sensors can determine an object's position based on its geometric position. UWB positioning systems use a combination of fixed anchors (reference points with known locations) and mobile tags (attached to objects being tracked) to determine precise real-time locations [35]. The system measures the time it takes for UWB radio signals to travel between the tags and anchors, a method known as Time-of-Flight (ToF) or Two-Way Ranging (TWR). By calculating these distances from multiple anchors (typically at least three for 2D or four for 3D positioning), the system uses trilateration to pinpoint the exact location of the tag. The problem that arises in this method is that the measurement results are imperfect. The measurement results are influenced by noise, which causes the measurement data to have deviations from the actual results. Therefore, estimating the measurement results to produce values close to the exact values is important.

The use of UWB sensors in localization methods is often susceptible to noise, drift, and external disturbances, resulting in significant estimation inaccuracies [36], [37]. Therefore, the Kalman filter is widely used in position estimation applications. The Kalman Filter is an optimal recursive estimation algorithm that efficiently predicts the state of a dynamic system from noisy measurements by combining prior knowledge with real-time data in a predictor-corrector loop. There are various issues associated with UWB sensors and the usefulness of the data they provide [38], [39]. Environmental

changes, geographical circumstances, and obstacles can all have an impact on the data's usefulness. Based on this, UWB sensor results may contain noise or mistakes, affecting data accuracy.

To overcome the inherent noise and imperfections in sensor-based localization systems, the Kalman Filter is regarded as one of the most effective and extensively used methods for filtering noisy data [40], [41]. It acts in two steps: prediction and correction. In the prediction stage, the Kalman Filter uses a mathematical model to predict the system's future state. In the correction stage, this estimate is updated using the most recent sensor readings, taking into account their uncertainty. This continual refining process enables the Kalman Filter to reduce estimation errors, making it perfect for real-time applications such as indoor localization via UWB, where accuracy and dependability are critical. Comparative studies have shown that Kalman Filters outperform traditional filtering methods such as moving average and low-pass filters, particularly in dynamic environments where rapid and accurate updates are essential.

Despite its benefits, the Kalman Filter's effectiveness is heavily reliant on the precise tuning of its process noise covariance (Q) and measurement noise covariance (R) variables [42]–[44]. Poorly chosen values might result in sluggish convergence, instability, or erroneous estimates. Fixed Q and R values may function well in controlled contexts, but suffer under the variable noise circumstances seen in real-world scenarios, according to research. Manually adjusting these settings is both time-consuming and inflexible [45]. As a result, researchers have explored various adaptive techniques, including machine learning [46] and heuristic optimization [47], [48], but many of these approaches are computationally expensive or not suitable for real-time applications.

One promising solution for adaptive tuning is the integration of Fuzzy Logic systems. Fuzzy Logic provides a flexible, rule-based framework capable of handling uncertainty and nonlinearities in complex systems [49], [50]. By monitoring the filter's estimation errors and system dynamics, a Fuzzy system can intelligently adjust the Q and R parameters of the Kalman Filter in real time. Compared to other adaptive methods [51]–[55], Fuzzy Logic offers a balance between adaptability and computational efficiency. Studies comparing Fuzzy-adaptive Kalman Filters with conventional and other adaptive methods (such as Genetic Algorithms and Particle Swarm Optimization) have shown that Fuzzy Logic-based tuning achieves superior tracking accuracy and faster convergence with lower computational cost [56], [57]. This makes the Kalman Filter combined with Fuzzy Logic a highly effective solution for enhancing the accuracy and robustness of UWB-based indoor localization systems.

This research contributes to designing and implementing Fuzzy Logic in Kalman Filter as adaptive tuning to determine the value of Q and R parameters in handling dynamic UWB sensor reading conditions. In addition, this study utilizes the Kalman Filter to improve the accuracy of determining the coordinates of the UWB sensor position in indoor areas based on the Trilateration method.

2. Method

This study aims to improve the accuracy of Ultra-Wideband (UWB) sensor readings in determining positional coordinates in indoor environments. The research block diagram can be seen in Fig. 1. This study uses three UWB sensors, with two sensors as anchors and one as a tag. The tag sensor is a mobile sensor representing a moving object in the indoor environment. The anchor sensors are fixed sensors that receive signals from the tag sensor and convert them into distance values.

2.1. Ultra-Wideband Sensor Based Localization

This research employs UWB technology through an ESP32-integrated DW3000 module to measure precise distance between a reference point and a mobile target. UWB represents a short-range radio communication technology that facilitates highly accurate ranging and spatial awareness, offering enhanced reliability and security for wireless positioning applications. The technology operates

by transmitting nanosecond pulses across a wide frequency spectrum, enabling centimeter-level precision in distance measurement while maintaining robust performance in multipath environments.

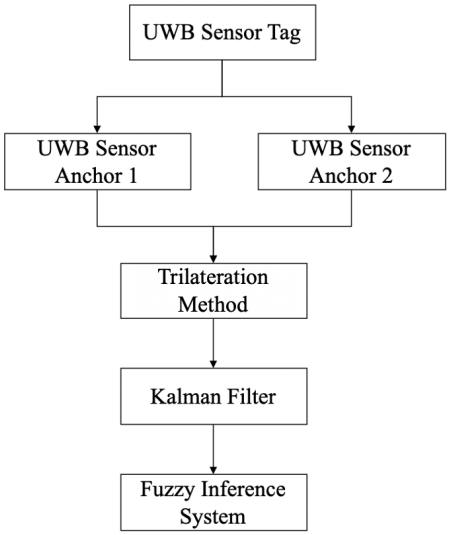

Fig. 1. Diagram block of research method

As shown in Fig. 1, this study uses 3 UWB sensors that function as anchors and tags. Anchors are generally fixed UWB devices with known locations. Tags generally refer to mobile UWB devices. Anchors and tags exchange information to determine the distance between them. The exact location of the tag can be determined by communicating with multiple anchors. UWB sensors utilize time-of-flight (ToF) measurements to determine the distance between devices, which allows for precise position and location tracking.

A geometric combination of anchor nodes and tag nodes is used to produce the position coordinates of the object. Fig. 2 shows two anchor nodes (node 1 and node 2) have a distance c. The distance between tag and node1 is defined as b. Meanwhile, the distance between tag and node 2 is defined as a. Distance c is a constant determined according to the robot design. Based on the Trilateration method, if the coordinates of node 1 are A (x_1,y_1) and node 2 are B (x_2,y_2), then the equation to find the position of the tag on C (x,y) can be seen in equations (1)-(5). The coordinates of C are at the intersection of two circles centered on A and B with the appropriate equations (1) and (2).

$$(x-x_1)^2+(y-y_1)^2=a^2 \tag{1}$$

$$(x-x_2)^2+(y-y_2)^2=b^2 \tag{2}$$

Subtracting the equations (1) and (2) produces the equation (3).

$$2x(x_2-x_1)+2y(y_2-y_1)=a^2-b^2+x_2^2+y_2^2-x_1^2-y_1^2 \tag{3}$$

In the condition $y_1=y_2$, then from (3) the value of x is obtained according to equation (4).

$$x=\frac{a^2-b^2+x_2^2-x_1^2}{2(x_2-x_1)} \tag{4}$$

By substituting (4) into equation (1), we get the value of y which is simplified to equation (5).

$$y=y_1\pm\sqrt{a^2-\left(\frac{a^2-b^2+(x_2-x_1)^2}{2(x_2-x_1)}\right)^2} \tag{5}$$

Therefore, the tag coordinates or C are obtained from equations (4) and (5).

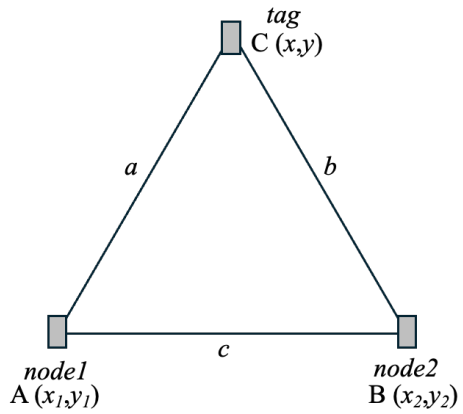

Fig. 2. Geometric combination of tag and anchor nodes

2.2. Kalman Filter

The Ultra-Wideband sensor's distance measurements suffer from low accuracy due to noise interference. To improve precision in determining object coordinates in indoor environment, a Kalman Filter (KF) algorithm is implemented. Kalman Filter is an algorithm for estimating the state of a system. This algorithm is carried out by combining measurements accompanied by noise from sensors and predictions from the process model. The Kalman filter uses two process stages, prediction and correction, to produce optimal state estimates.

The model-based prediction stage functions to propagate the state vector into the future using a linear model. The correction stage combines current predictions with current measurement results to obtain the corrected estimated state. The prediction equation can be seen in (6) and (7). Equation (6) shows the predicted state estimation, and (7) shows the predicted error covariance.

$$\hat{x}_{k|k-1} = F_k \hat{x}_{k-1|k-1} + B_k u_k \tag{6}$$

$$P_{k|k-1} = F_k P_{k-1|k-1} F_k^T + Q_k \tag{7}$$

The predicted state estimate $\hat{x}_{k|k-1}$ represents the a priori estimation of x at time step k, calculated using all available observations up to the previous time step $k-1$. This prediction is accompanied by its corresponding error covariance matrix $P_{k|k-1}$, which characterizes the uncertainty in the state estimate by projecting the expected accuracy based on measurements through $k-1$. Together, these predicted quantities form the Kalman Filter's forward estimation step, where $\hat{x}_{k|k-1}$ provides the best available state prediction. At the same time, $P_{k|k-1}$ quantifies the confidence in this prediction before incorporating new measurements at time k.

According to equation (6), state transition model (F_k) applied in previous state x_{k-1}. Control input model (B_k) is applied to control vector (u_k). The state transition matrix F_k projects the previous covariance ($P_{k-1|k-1}$) to the current time step, while Q_k represents the process noise covariance matrix that captures uncertainties arising from external disturbances or model imperfections. The term $F_k P_{k-1|k-1} F_k^T$ preserves the uncertainty structure from the prior estimate, whereas Q augments this uncertainty to reflect accumulated prediction errors. Consequently, $P_{k|k-1}$ quantitatively measures the confidence in the state prediction ($\hat{x}_{k|k-1}$) prior to the assimilation of new measurement data. This matrix plays a critical role in determining the Kalman Gain (K_k), which optimally balances the weighting between model predictions and actual observations. When $P_{k|k-1}$ is large, the filter places greater trust in the measurements. On the other hand, when small, it relies more heavily on the model prediction.

The update equation can be seen in equations (8)-(12). The three main components in this process are the calculation of the Kalman gain (K_k) in equation (10), the update of the state estimate ($\hat{x}_{k|k}$) in equation (11), and the update of the error covariance matrix ($P_{k|k}$) in equation (12). The Kalman gain optimally balances the weights between model predictions and actual measurements based on their uncertainties. The H_k matrix is an observation matrix that maps the states to measurement domains, while R_k represents the measurement noise covariance. The updated estimate state ($\hat{x}_{x|x}$) is combined with the innovation ($\tilde{y}$) that reflects the difference between the actual (z_k) and predicted measurements. After incorporating new measurement information, the error covariance matrix is updated to reduce the estimation uncertainty.

$$\tilde{y}_k = z_k + K_k \hat{x}_{k|k-1} \tag{8}$$

$$S_k = H_k P_{k-1|k-1} H_k^T + R_k \tag{9}$$

$$K_k = P_{k|k-1} H_k^T S_k^{-1} \tag{10}$$

$$\hat{x}_{k|k} = \hat{x}_{k|k-1} + K_k \tilde{y}_k \tag{11}$$

$$P_{k|k} = (I - K_k H_k) P_{k|k-1} \tag{12}$$

This research utilizes Ultra-Wideband sensors to measure real-time distances, where the raw distance measurement at time step k is denoted as z_k. The Kalman Filter is applied to process these measurements, combining the system's dynamic model (with process noise covariance Q_k) and sensor noise characteristics (measurement noise covariance R_k) to produce more accurate distance estimates ($\hat{x}_{k|k}$). By iteratively predicting and correcting the state, the filter reduces the impact of UWB-specific errors such as multipath interference and signal noise. The refined output demonstrates improved stability and precision compared to raw sensor data, making it suitable for indoor localization.

2.3. Fuzzy Logic

A critical limitation of the standard Kalman Filter lies in its reliance on fixed Q_k and R_k values, which assume constant noise statistics throughout operation. In real-world UWB applications, environmental dynamics, such as signal obstruction, moving obstacles, or interference, can cause time-varying noise levels that fixed values cannot adapt to. These constraints highlight the need for an adaptive approach to noise modelling in dynamic UWB-based systems. This study proposes a fuzzy logic-based adaptive mechanism to dynamically adjust Q_k and R_k based on real-time conditions to address these limitations.

The input of fuzzy logic in the form of error (e_k) and measurement difference/ delta measurements (Δz_k) can be seen in equations (13) and (14), respectively. The system error is obtained from the difference between the current sensor measurement value and the estimated state at the previous time step. On the other hand, delta measurements are obtained from the difference between the current measurement value and the previous measurement result. The delta measurement value is used to see the level of change in the measurement results produced by the Ultra-Wideband sensor.

$$e_k = z_k - \hat{x}_{k-1|k-1} \tag{13}$$

$$\Delta z_k = z_k - z_{k-1} \tag{14}$$

The Fuzzy Logic block diagram is shown in Fig. 3. The inputs in the form of e_k and Δz_k, which are crisp, are converted to fuzzy values through the fuzzification process in the fuzzification inference unit. The error range is categorized into three fuzzy membership functions corresponding to negative, zero, and positive error states. The membership function of the input error can be seen in (15) to (17). The graphical form representing the membership function of error can be seen in Fig. 4(a).

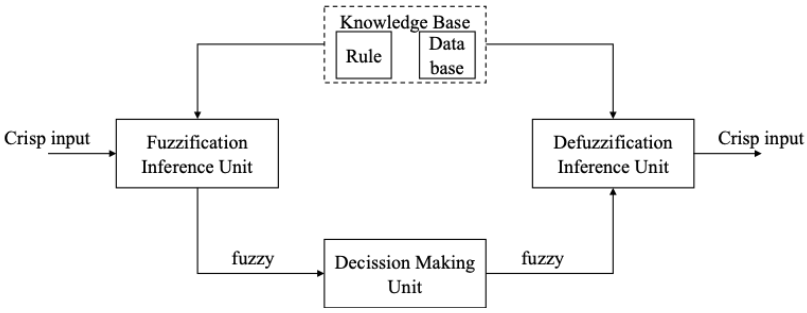

Fig. 3. The block diagram of fuzzy logic

$$\mu_{negative}(x_i) = \begin{cases} 1 & \text{if } x_i < -3 \\ \frac{-x_i - 0.1}{2.9} & \text{if } -3 \leq x_i \leq -0.1 \\ 0 & \text{if } x > -0.1 \end{cases} \tag{15}$$

$$\mu_{zero}(x_i) = \begin{cases} 0 & \text{if } x_i < -0.5 \\ \frac{x_i + 0.5}{0.5} & \text{if } -0.5 \leq x_i \leq 0 \\ \frac{0.5 - x_i}{0.5} & \text{if } 0 < x_i \leq 0.5 \\ 0 & \text{if } x_i > 0.5 \end{cases} \tag{16}$$

$$\mu_{positive}(x_i) = \begin{cases} 0 & \text{if } x_i < 0.1 \\ \frac{x_i - 0.1}{2.9} & \text{if } 0.1 \leq x_i \leq 3 \\ 1 & \text{if } x > 3 \end{cases} \tag{17}$$

The delta measurement values are classified into three categories: decreasing, steady, and increasing values. The membership functions for the input delta measurements are presented in equations (18) to (20). The graphical form representing the membership function of delta measurements can be seen in Fig. 4(b).

$$\mu_{decreasing}(x_i) = \begin{cases} 1 & \text{if } x_i < -11 \\ \frac{-x_i - 0.7}{0.3} & \text{if } -1 \leq x_i \leq 0.2 \\ 0 & \text{if } x > 0.2 \end{cases} \tag{18}$$

$$\mu_{steady}(x_i) = \begin{cases} 0 & \text{if } x_i < 0 \\ \frac{x_i}{0.5} & \text{if } 0 \leq x_i \leq 0.5 \\ \frac{1 - x_i}{0.5} & \text{if } 0.5 < x_i \leq 0.1 \\ 0 & \text{if } x_i > 1 \end{cases} \tag{19}$$

$$\mu_{increasing}(x_i) = \begin{cases} 0 & \text{if } x_i < 0.8 \\ \frac{x_i - 0.8}{1.2} & \text{if } 0.8 \leq x_i \leq 2 \\ 1 & \text{if } x > 2 \end{cases} \tag{20}$$

A fuzzy-based adaptation mechanism is developed to dynamically adjust the process noise covariance (Q_k) and measurement noise covariance (R_k) matrices. The output membership functions for both parameters are defined through three triangular fuzzy sets (small, medium, large), with mathematical representations provided in Equations (21)-(23) for Q_k and (24)-(26) for R_k. Visualizations

of these membership functions appear in Fig. 4(b-c).

$$\mu_{small}(x_i) = \begin{cases} 1 & \text{if } x_i < 0 \\ \frac{0.8-x_i}{0.8} & \text{if } 0 \leq x_i \leq 0.8 \\ 0 & \text{if } x > 0.8 \end{cases} \tag{21}$$

$$\mu_{medium}(x_i) = \begin{cases} 0 & \text{if } x_i < 0.5 \\ \frac{x_i-0.5}{0.5} & \text{if } 0.5 \leq x_i \leq 1 \\ \frac{1.5-x_i}{0.5} & \text{if } 1 < x_i \leq 1.5 \\ 0 & \text{if } x_i > 1.5 \end{cases} \tag{22}$$

$$\mu_{large}(x_i) = \begin{cases} 0 & \text{if } x_i < 1.2 \\ \frac{x_i-1.2}{0.8} & \text{if } 1.2 \leq x_i \leq 2 \\ 1 & \text{if } x > 2 \end{cases} \tag{23}$$

$$\mu_{small}(x_i) = \begin{cases} 1 & \text{if } x_i < 0 \\ \frac{40-x_i}{40} & \text{if } 0 \leq x_i \leq 40 \\ 0 & \text{if } x > 40 \end{cases} \tag{24}$$

$$\mu_{medium}(x_i) = \begin{cases} 0 & \text{if } x_i < 30 \\ \frac{x_i-30}{20} & \text{if } 30 \leq x_i \leq 50 \\ \frac{70-x_i}{20} & \text{if } 50 < x_i \leq 70 \\ 0 & \text{if } x_i > 70 \end{cases} \tag{25}$$

$$\mu_{large}(x_i) = \begin{cases} 0 & \text{if } x_i < 60 \\ \frac{x_i-100}{40} & \text{if } 60 \leq x_i \leq 100 \\ 1 & \text{if } x > 100 \end{cases} \tag{26}$$

Fuzzy Logic rules based on the input and output defined above can be seen in Table 1. These rules are used to make decisions about the Q_k and R_k values in the system. This study uses the Mamdani Fuzzy Inference System (FIS) as the central part of the decision-making unit.

According to Fig. 3, the final stage of Fuzzy Logic is defuzzification. In the defuzzification process, the output values of Q_k and R_k, which are fuzzy values, are changed into crisp form. The method used in defuzzification is the centroid. The centoid or center of gravity method uses the total area of the membership function distribution to show the combined control action divided into several small areas. Each area is then calculated for its area and center of mass, then the summation of all areas is carried out to obtain the defuzzification value on the discrete fuzzy set. The defuzzification value (x^*) using the centroid method can be seen in equation (27).

$$x^* = \frac{\sum_{i=1}^{n} x_i \mu(x_i)}{\sum_{i=1}^{n} \mu(x_i)} \tag{27}$$

3. Result and Discussion

The first research result analyses the error produced by the Ultra-Wideband (UWB) sensor compared to the actual distance/ real value. Fig. 5 compares the UWB sensor's measured values and the standard reference measurements. Fig. 5 indicates that the UWB sensor's distance measurements do not exhibit stable values and tend to fluctuate.

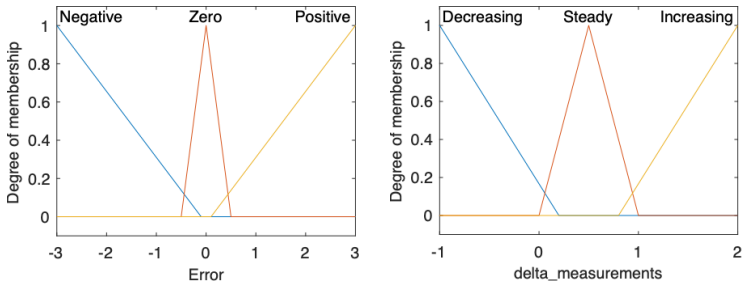

(a) Input error (b) Input delta measurements

(c) Output Q value (d) Output R value

Fig. 4. Membership function of each variable

The performance evaluation of the UWB sensor for distance measurement was conducted using two evaluation metrics: Mean Absolute Error (MAE) and Root Mean Squared Error (RMSE). MAE measures the average absolute error between the sensor's predicted values and the actual distance, providing an accuracy assessment without being affected by error direction (positive/negative). This metric is handy for evaluating sensor consistency, especially in environments with multipath interference or random noise, as it is less sensitive to outliers. Meanwhile, RMSE offers a stricter perspective by squaring the errors before averaging them, thereby giving higher weight to significant errors (such as outliers or anomalies). The equations for MAE and RMSE can be seen in equations (28) and (29).

$$MAE = \frac{1}{N}\sum_{k=1}^{N}\left|v_k - \hat{x}_{k|k-1}\right| \tag{28}$$

$$RMSE = \sqrt{\frac{1}{N}\sum_{k=1}^{N}(v_k - \hat{x}_{k|k-1})^2} \tag{29}$$

where N is the total amount of data, v_k is the actual value or true value, and $\hat{x}_{k|k-1}$ is the estimation value of the model.

Table 1. Rules of fuzzy logic

No.	Input of Fuzzy Logic		Output of Fuzzy Logic	
	Error	Delta Measurements	Q_k	R_k
1	negative	decreasing	large	small
2	negative	steady	medium	small
3	negative	increasing	small	small
4	zero	decreasing	medium	medium
5	zero	steady	small	medium
6	zero	increasing	small	large
7	positive	decreasing	small	small
8	positive	steady	small	medium
9	positive	increasing	small	large

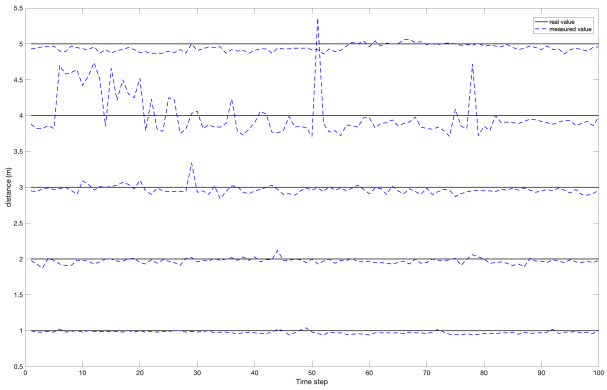

Fig. 5. Comparison of measured to true values

Table 2 shows the MAE and RMSE values based on the results of sensor distance measurements at 1m - 5m. The measurement results show that the UWB sensor has a smaller MAE than the RMSE. This indicates that, on average, the sensor has quite good accuracy. However, there are several measurements with significant errors (outliers). A low MAE suggests that most of the measurement data is close to the true/real value with a slight deviation. A higher RMSE value indicates several measurements with significant errors, which may be caused by environmental noise interference.

The difference between MAE and RMSE indicates that the UWB system is still susceptible to anomalies, so further optimization is needed to improve the reliability of the measurement.

Table 2. UWB performance in generating distance data

Distance (m)	MAE (m)	RMSE (m)
1	0.0257	0.0300
2	0.0362	0.0460
3	0.0521	0.0680
4	0.2133	0.2927
5	0.0623	0.0734

The application of the Kalman Filter can be an effective solution to reduce the influence of noise and outliers on UWB measurements. The Kalman Filter utilizes sensor data to produce a more stable estimate. By combining noisy UWB measurements with model predictions, the Kalman Filter can smooth the data, reduce error variance, and eliminate outliers. In addition, this filter is also able to compensate for measurement delays and improve system response in real time. Implementing the Kalman Filter on the UWB sensor is expected to reduce the RMSE close to the MAE value, reducing measurement instability while maintaining average accuracy.

The results of the study according to Table 3 show that the application of the Kalman Filter and Fuzzy Kalman Filter can significantly reduce the MAE and RMSE values compared to the raw data of UWB sensor measurements. This decrease indicates that both filtering methods have reduced noise and measurement instability, thereby increasing system accuracy. In particular, the RMSE, which tends to approach the MAE value after signal processing, indicates that the error distribution becomes more concentrated around the average value, with few outliers or significant errors.

This proves that the filter used improves precision and measurement consistency, making the system more reliable in real-time applications such as autonomous navigation or object tracking. Furthermore, the results of the study revealed that the MAE and RMSE values of the conventional Kalman Filter are greater than those of the Fuzzy Kalman Filter.

Table 3. Comparison of UWB performance in generating distance data using kalman filter and fuzzy kalman filter

Distance	Kalman Filter		Fuzzy Kalman Filter	
(m)	MAE (m)	RMSE (m)	MAE (m)	RMSE (m)
1	0.0236	0.0276	0.0211	0.0242
2	0.0326	0.0387	0.0266	0.0288
3	0.0446	0.0530	0.0455	0.0388
4	0.1765	0.2313	0.1142	0.1402
5	0.0606	0.0703	0.0575	0.0657

This difference is due to the ability of the Fuzzy Kalman Filter to adjust the noise (Q_k) and measurement noise (R_k) process parameters adaptively based on dynamic environmental conditions. While Kalman Filter uses fixed Q_k and R_k values, Fuzzy Kalman Filter utilizes fuzzy logic to optimize these parameters in real-time, making it more responsive to noise.

This adaptability results in more accurate estimations, as reflected by the decrease in MAE and RMSE value of Fuzzy Kalman Filter. Thus, the integration of fuzzy logic into the Kalman Filter improves the system's robustness to noise variations and enhances the measurement stability, making it a better solution for UWB sensor applications in complex and dynamic environments.

The visualization of measurement results comparing the Kalman Filter and Fuzzy Kalman Filter is presented in Fig. 6. The graph demonstrates that the Fuzzy Kalman Filter exhibits better performance in reducing noise and enhancing signal stability than the conventional Kalman Filter. This improvement is attributed to the adaptive nature of the Fuzzy Kalman Filter, which dynamically adjusts its parameters to better handle uncertainties in the system. Both algorithms were tested using initial $Q_k = 1$ and $R_k = 1$, ensuring a fair comparison under identical starting conditions.

Despite these initial settings, the Fuzzy Kalman Filter consistently outperforms its traditional counterpart, particularly in scenarios with high variability or unpredictable noise patterns. Fig. 7 illustrates the adaptive values of $Q_k = 1$ and $R_k = 1$ in the Fuzzy Kalman Filter, indicating the algorithm's ability to self-adjust and optimize its performance in real-time. This adaptability is a key advantage, as it eliminates manual tuning of these parameters, which is often a challenging and time-consuming in the standard Kalman Filter.

The Fuzzy Kalman Filter visually produces more stable sensor readings, as evidenced by the smoother output curve in Fig. 1. This stability is achieved without requiring prior adjustment of $Q_k = 1$ and $R_k = 1$, highlighting the algorithm's robustness and practicality for real-world applications where noise characteristics may not be known in advance. The last experiment was conducted using three UWB sensors. Two distance data generated by the UWB sensor were fed into the Fuzzy Kalman Filter to obtain more accurate results. The two datasets were processed into position coordinates from the UWB sensor, which were used as tags according to the x and y equations. The results of the 2D coordinates from the calculation were also filtered using the Kalman Filter with fixed Q and R values of 0.1 and 100.

The results of the position coordinate distribution are shown in Fig. 8. Based on Fig. 8, the position coordinates of the anchor reading results filtered using the Fuzzy Kalman Filter still show a wide distribution, even though the distance accuracy has increased when compared to the desired coordinate value. This is different from the results of the position coordinates using the Kalman Filter, which are more precise. According to Table 4, the average value of RMSE and MSE represents the correct position coordinates against the unfiltered position coordinates and with the Kalman Filter. The average value of RMSE and MAE of the actual position error against the unfiltered position is 1.0916 and 0.8406. This shows that the position estimation system is accurate with a mean absolute error (MAE) below 1 meter. Some significant errors cause a higher RMSE, indicating inconsistent performance.

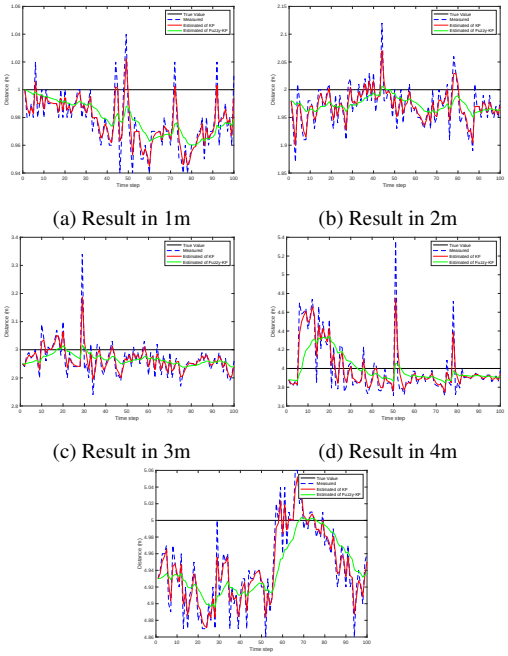

(a) Result in 1m (b) Result in 2m

(c) Result in 3m (d) Result in 4m

(e) Result in 5m

Fig. 6. Visualization of the comparison of UWB sensor measurement performance against true values.

The difference between RMSE and MAE suggests the presence of outliers or points with substantial deviations.

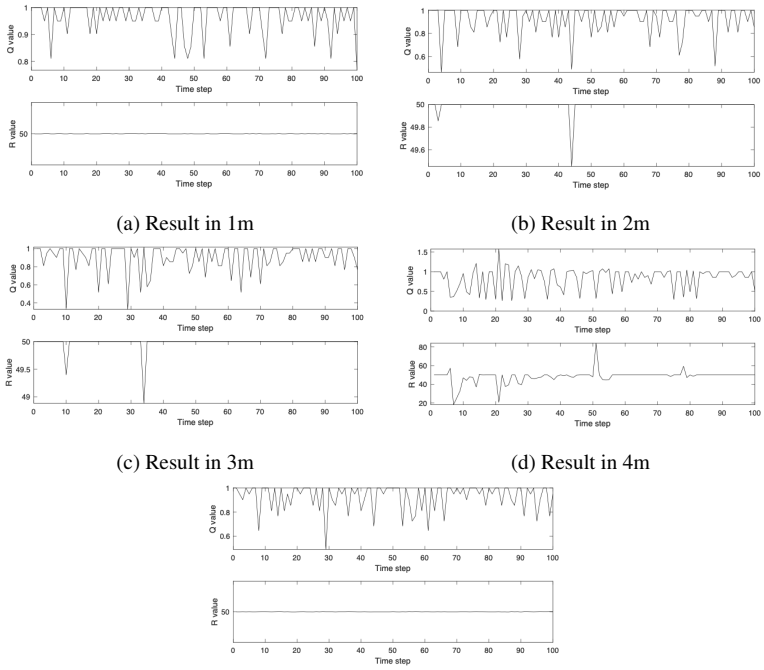

(a) Result in 1m (b) Result in 2m

(c) Result in 3m (d) Result in 4m

(e) Result in 5m

Fig. 7. Changes in the values of the Q_k and R_k parameters in the Fuzzy Kalman Filter

Table 4. Comparison of system performance in determining position coordinates with and without filters

Coordinates (m)	Without Filter		With Filter	
	MAE (m)	RMSE (m)	MAE (m)	RMSE (m)
(0.87 , 3.50)	0.6418	0.8372	0.4148	0.4154
(0.35 , 4.40)	0.8697	1.1753	0.1047	0.1050
(2.00 , 6.00)	1.1100	1.3837	0.6198	0.6206
(0.11 , 2.30)	0.4707	0.5760	0.1085	0.1086
(0.35 , 4.98)	1.1109	1.4855	0.6763	0.6770

On the other hand, the average results of RMSE and MAE of the correct position error against the filtered position are 0.3853 and 0.3848. This shows that the position estimation model using the Kalman Filter has a high level of accuracy, indicating that the average position estimation error against the actual position is less than 0.39 meters.

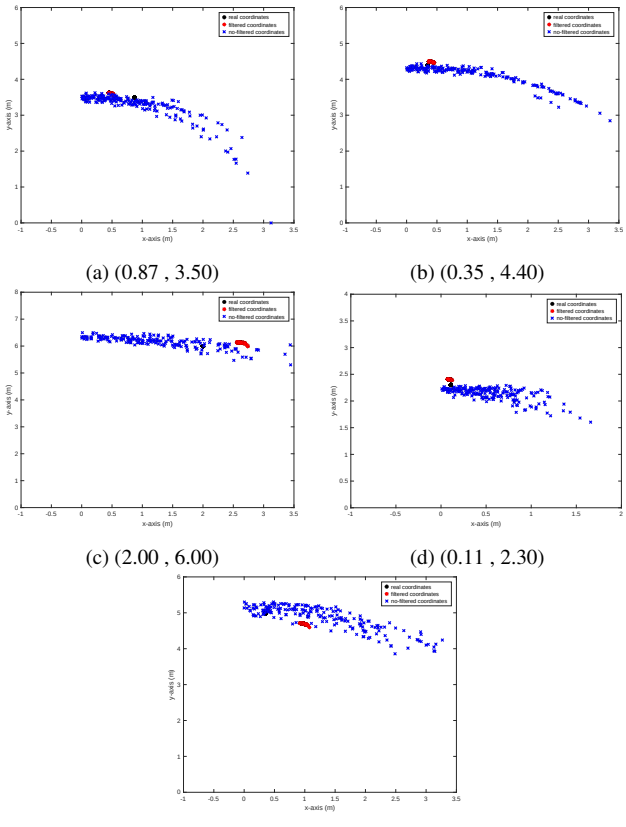

(a) (0.87 , 3.50) (b) (0.35 , 4.40)

(c) (2.00 , 6.00) (d) (0.11 , 2.30)

(e) (0.35 , 4.98)

Fig. 8. Coordinates distribution of tag sensor

These two nearly identical values suggest that the distribution of estimation errors is very consistent, with no outliers or significant errors, since the RMSE, which is sensitive to high deviations, is only slightly different from the MAE.

This reflects that the model works stably and precisely across a wide range of measurement points, both under ideal conditions and those that may contain minimal noise.

4. Conclusion

Based on the evaluation results, the implementation of Fuzzy Kalman Filter (FKF) has been proven to be effective in improving estimation accuracy by significantly reducing the mean absolute error (MAE) and root mean square error (RMSE). The decrease in MAE indicates that the average absolute error in the estimation is getting smaller. At the same time, the decrease in RMSE shows an increase in precision and a reduction in error variability.

This proves that integrating fuzzy logic and the Kalman Filter can better overcome system uncertainty and nonlinear noise than conventional methods. Thus, FKF improves estimation accuracy and reduces error dispersion, resulting in more stable and reliable predictions. Furthermore, the greater decrease in RMSE compared to MAE indicates that FKF successfully minimizes outliers or extreme deviations in the estimation data.

This implies that the fuzzy approach in Kalman Filter parameter adaptation can dynamically adjust to data fluctuations, thereby reducing the overall error range. These findings have important implications in developing adaptive estimation systems, especially in environments with high noise and non-linear dynamics.

Author Contribution: All authors contributed equally to the main contributor to this paper. All authors read and approved the final paper.

Acknowledgement: Author would like to express special gratitude and thanks to Universitas Ahmad Dahlan for research grants with contract number: 002/IRMG/LPPM-UAD/IX/2024.

Conflicts of Interest: The authors declare no conflict of interest.

References

[1] I. Hroob, S. Molina, R. Polvara, G. Cielniak, and M. Hanheide, "Adaptive robot localization in dynamic environments through self-learnt long-term 3D stable points segmentation," *Robotics and Autonomous Systems*, vol. 181, p. 104786, 2024, https://doi.org/10.1016/j.robot.2024.104786.

[2] A. Yarovoi and Y. K. Cho, "Review of simultaneous localization and mapping (SLAM) for construction robotics applications," *Automation in Construction*, vol. 162, p. 105344, 2024, https://doi.org/10.1016/j.autcon.2024.105344.

[3] S. Lafuente-Arroyo, S. Maldonado-Bascón, D. Delgado-Mena, C. Gutiérrez-Álvarez, and F. J. Acevedo-Rodríguez, "Multisensory integration for topological indoor localization of mobile robots in complex symmetrical environments," *Expert Systems with Applications*, vol. 241, p. 122561, 2024, https://doi.org/10.1016/j.eswa.2023.122561.

[4] A. Le Floch, R. Kacimi, P. Druart, Y. Lefebvre, and A.-L. Beylot, "A comprehensive framework for 5G indoor localization," *Computer Communications*, vol. 228, p. 107968, 2024, https://doi.org/10.1016/j.comcom.2024.107968.

[5] C. Sun, R. van der Tol, R. Melenhorst, L. A. P. Pacheco, and P. G. Koerkamp, "Path planning of manure-robot cleaners using grid-based reinforcement learning," *Computers and Electronics in Agriculture*, vol. 226, p. 109456, 2024, https://doi.org/10.1016/j.compag.2024.109456.

[6] J. Kim, "Autonomous robot vacuum system composed of a cleaner robot and a dust storage robot," *Journal of the Franklin Institute*, vol. 361, no. 11, p. 106938, 2024, https://doi.org/10.1016/j.jfranklin.2024.106938.

[7] N. Stoimenov, P. Stoev, N. Chivarov, and G. Kotseva, "Path Simulation Methodology for Robotic Cleaning Systems in Animal Husbandry," *IFAC-PapersOnLine*, vol. 55, no. 39, pp. 447–451, 2022, https://doi.org/10.1016/j.ifacol.2022.12.078.

[8] M. Cornet, R. D. S. Tchilian, and M. Netto, "A swarm of luggage transport robots moving through an airport," *IFAC-PapersOnLine*, vol. 55, no. 2, pp. 102–107, 2022, https://doi.org/10.1016/j.ifacol.2022.04.177.

[9] V. A. Silva, M. P. Roriz Junior, and M. C. G. da S. P. Bandeira, "Detecting airport luggage dimensions through low-cost depth sensors," *Journal of Air Transport Management*, vol. 119, p. 102649, 2024, https://doi.org/10.1016/j.jairtraman.2024.102649.

[10] A. Zachariae, F. Plahl, Y. Tang, I. Mamaev, B. Hein, and C. Wurll, "Human-robot interactions in autonomous hospital transports," *Robotics and Autonomous Systems*, vol. 179, p. 104755, 2024, https://doi.org/10.1016/j.robot.2024.104755.

[11] P. Stoev, R. Ficherov, and M. Georgiev, "Development of a Mobile Robot for Distribution of Medicine in Hospitals," *IFAC-PapersOnLine*, vol. 58, no. 3, pp. 221–225, 2024, https://doi.org/10.1016/j.ifacol.2024.07.154.

[12] Y. Gong, J. Seo, T. W. Kim, S. Ahn, and Y. Luo, "Field validation of beacon-based indoor tracking and localization system for construction workers," *KSCE Journal of Civil Engineering*, vol. 29, no. 2, p. 100017, 2025, https://doi.org/10.1016/j.kscej.2024.100017.

[13] S. I. Khan, B. R. Ray, and N. C. Karmakar, "RFID localization in construction with IoT and security integration," *Automation in Construction*, vol. 159, p. 105249, 2024, https://doi.org/10.1016/j.autcon.2023.105249.

[14] W. Liu, M. Niu, and Y. S. Han, "RIFi: Robust and iterative indoor localization based on Wi-Fi RSS fingerprints," *Journal of Information and Intelligence*, vol. 3, no. 1, pp. 1–18, 2025, https://doi.org/10.1016/j.jiixd.2024.07.003.

[15] Y. Liang, S. Chen, X. Dong, and T. Liu, "Fine-grained grid computing model for Wi-Fi indoor localization in complex environments," *Journal of Electronic Science and Technology*, vol. 22, no. 1, p. 100234, 2024, https://doi.org/10.1016/j.jnlest.2024.100234.

[16] A. A. Morgan, "On the accuracy of BLE indoor localization systems: An assessment survey," *Computers and Electrical Engineering*, vol. 118, p. 109455, 2024, https://doi.org/10.1016/j.compeleceng.2024.109455.

[17] K. Szyc, M. Nikodem, and M. Zdunek, "Bluetooth low energy indoor localization for large industrial areas and limited infrastructure," *Ad Hoc Networks*, vol. 139, p. 103024, 2023, https://doi.org/10.1016/j.adhoc.2022.103024.

[18] Y. Wang, Y. Zhou, Y. Lu, and C. Cui, "MSTSCKF-based INS/UWB integration for indoor localization," *Ain Shams Engineering Journal*, vol. 15, no. 10, p. 102939, 2024, https://doi.org/10.1016/j.asej.2024.102939.

[19] C. Tu, J. Zhang, Z. Quan, and Y. Ding, "UWB indoor localization method based on neural network multi-classification for NLOS distance correction," *Sensors and Actuators A: Physical*, vol. 379, p. 115904, 2024, https://doi.org/10.1016/j.sna.2024.115904.

[20] P. Janousek, Z. Slanina, and W. Walendziuk, "Target-following Robotic Platform Based on UWB Localization and Depth Camera," *IFAC-PapersOnLine*, vol. 58, no. 9, pp. 247–252, 2024, https://doi.org/10.1016/j.ifacol.2024.07.404.

[21] D. Hettiarachchi, Y. Tian, H. Yu, and S. Kamijo, "Depth as attention to learn image representations for visual localization, using monocular images," *Journal of Visual Communication and Image Representation*, vol. 98, p. 104012, 2024, https://doi.org/10.1016/j.jvcir.2023.104012.

[22] Q. Li, Y. Zhuang, and J. Huai, "Multi-sensor fusion for robust localization with moving object segmentation in complex dynamic 3D scenes," *International Journal of Applied Earth Observation and Geoinformation*, vol. 124, p. 103507, 2023, https://doi.org/10.1016/j.jag.2023.103507.

[23] B. Van Herbruggen et al., "Strategy analysis of badminton players using deep learning from IMU and UWB wearables," *Internet of Things*, vol. 27, p. 101260, 2024, https://doi.org/10.1016/j.iot.2024.101260.

[24] M. Zhang, L. Ma, K. Shen, and Y. Sun, "Autonomous Localization and Motion Control of Under-Vehicle Inspection Robot," *IFAC-PapersOnLine*, vol. 56, no. 2, pp. 3060–3065, 2023, https://doi.org/10.1016/j.ifacol.2023.10.1435.

[25] S. Wu, S. Huang, Z. Liu, Q. Zhang, and J. Liu, "AFPILD: Acoustic footstep dataset collected using one microphone array and LiDAR sensor for person identification and localization," *Information Fusion*, vol. 104, p. 102181, 2024, https://doi.org/10.1016/j.inffus.2023.102181.

[26] M. Y. Tsai and F. C. Tsai, "Utilizing Multiple Condition RSSI Distance Conversion on WiFi Localization," *Procedia Computer Science*, vol. 246, pp. 5304–5311, 2024, https://doi.org/10.1016/j.procs.2024.09.645.

[27] A. S. Lutakamale, H. C. Myburgh, and A. de Freitas, "RSSI-based fingerprint localization in LoRaWAN networks using CNNs with squeeze and excitation blocks," *Ad Hoc Networks*, vol. 159, p. 103486, 2024, https://doi.org/10.1016/j.adhoc.2024.103486.

[28] A. H. M. Kamal, M. G. R. Alam, M. R. Hassan, T. S. Apon, and M. M. Hassan, "Explainable indoor localization of BLE devices through RSSI using recursive continuous wavelet transformation and XGBoost classifier," *Future Generation Computer Systems*, vol. 141, pp. 230–242, 2023, https://doi.org/10.1016/j.future.2022.11.001.

[29] J. Jankkari, M. Kutila, and A. Virtanen, "Evaluation of UWB based Automated Vehicle Positioning," *Transportation Research Procedia*, vol. 72, pp. 56–63, 2023, https://doi.org/10.1016/j.trpro.2023.11.322.

[30] M. Munadi, B. Radityo, M. Ariyanto, and Y. Taniai, "Automated guided vehicle (AGV) lane-keeping assist based on computer vision, and fuzzy logic control under varying light intensity," *Results in Engineering*, vol. 21, p. 101678, 2024, https://doi.org/10.1016/j.rineng.2023.101678.

[31] A. Harindranath and M. Arora, "Effect of sensor noise characteristics and calibration errors on the choice of IMU-sensor fusion algorithms," *Sensors and Actuators A: Physical*, vol. 379, p. 115850, 2024, https://doi.org/10.1016/j.sna.2024.115850.

[32] M. Yusuf *et al*., "IoT-based low-cost 3D mapping using 2D Lidar for different materials," *Materialstoday: Proceedings*, vol. 57, pp. 942–947, 2022, https://doi.org/10.1016/j.matpr.2022.03.161.

[33] M. Guan and C. Wen, "Autonomous exploration using UWB and LiDAR," *Journal of Automation and Intelligence*, vol. 2, no. 1, pp. 51–60, 2023, https://doi.org/10.1016/j.jai.2022.100006.

[34] A. de Jesus Aragão, D. Carvalho, B. Sanches, and W. A. M. Van Noije, "Low-cost device for breast cancer screening: A dry setup IR-UWB proposal," *Biomedical Signal Processing and Control*, vol. 79, p. 104078, 2023, https://doi.org/10.1016/j.bspc.2022.104078.

[35] Q. Zhang, X. Xu, F. Shi, L. Shu, and J. Wang, "An integrated positioning method with IMU/UWB based on geometric constraints of foot-to-foot distances," *Measurement*, vol. 242, p. 115771, 2025, https://doi.org/10.1016/j.measurement.2024.115771.

[36] Z. Niu, H. Yang, L. Zhou, M. Farag Taha, Y. He, and Z. Qiu, "Deep learning-based ranging error mitigation method for UWB localization system in greenhouse," *Computers and Electronics in Agriculture*, vol. 205, p. 107573, 2023, https://doi.org/10.1016/j.compag.2022.107573.

[37] V. Yogesh, L. Grevinga, C. Voort, J. H. Buurke, P. H. Veltink, and C. T. M. Baten, "Novel calibration method for improved UWB sensor distance measurement in the context of application for 3D analysis of human movement," *Engineering Science and Technology, an International Journal*, vol. 58, p. 101844, 2024, https://doi.org/10.1016/j.jestch.2024.101844.

[38] Y. Li, Z. Gao, C. Yang, and Q. Xu, "A novel UWB/INS tight integration model based on ranging offset calibration and robust cubature Kalman filter," *Measurement*, vol. 237, p. 115186, 2024, https://doi.org/10.1016/j.measurement.2024.115186.

[39] Y. Wang, S. Fu, and F. Wang, "Improved maximum correntropy criterion Kalman filter with adaptive behaviors for INS/UWB fusion positioning algorithm," *Alexandria Engineering Journal*, vol. 109, pp. 702–714, 2024, https://doi.org/10.1016/j.aej.2024.09.065.

[40] Y. Zhang *et al*., "A method of eliminating the signal-dependent random noise from the raw CMOS image sensor data based on Kalman filter," *Signal Processing,* vol. 104, pp. 401–406, 2014, https://doi.org/10.1016/j.sigpro.2014.04.026.

[41] Z. Zhu and S. Zhu, "Asynchronous Kalman filtering for dynamic response reconstruction by fusing multi-type sensor data with arbitrary sampling frequencies," *Mechanical Systems and Signal Processing*, vol. 215, p. 111395, 2024, https://doi.org/10.1016/j.ymssp.2024.111395.

[42] K. Xiong, C. Wei, and H. Zhang, "Q-learning for noise covariance adaptation in extended KALMAN filter," *Asian Journal of Control*, vol. 23, no. 4, pp. 1803–1816, 2021, https://doi.org/10.1002/asjc.2336.

[43] K. Xiong, C. Wei, and P. Zhou, "Integrated autonomous optical navigation using Q-Learning extended Kalman filter," *Aircraft Engineering and Aerospace Technology: An International Journal*, vol. 94, no. 6, pp. 848–861, 2022, https://doi.org/10.1108/AEAT-05-2021-0139.

[44] H. Lan, J. Hu, Z. Wang and Q. Cheng, "Variational Nonlinear Kalman Filtering With Unknown Process Noise Covariance," in *IEEE Transactions on Aerospace and Electronic Systems*, vol. 59, no. 6, pp. 9177-9190, 2023, https://doi.org/10.1109/TAES.2023.3314703.

[45] D. Ćetenović, A. Ranković, J. Zhao, Z. Jin, J. Wu, and V. Terzija, "An adaptive method for tuning process noise covariance matrix in EKF-based three-phase distribution system state estimation," *International Journal of Electrical Power & Energy Systems*, vol. 132, p. 107192, 2021, https://doi.org/10.1016/j.ijepes.2021.107192.

[46] G. Liu, P. Neupane, H. -C. Wu, W. Xiang, L. Pu and S. Y. Chang, "Novel Robust Indoor Device-Free Moving-Object Localization and Tracking Using Machine Learning With Kalman Filter and Smoother," in *IEEE Systems Journal*, vol. 16, no. 4, pp. 6253-6264, 2022, https://doi.org/10.1109/JSYST.2022.3198069.

[47] L. Janjanam, S. Kumar Saha, R. Kar, and D. Mandal, "Optimal design of cascaded Wiener-Hammerstein system using a heuristically supervised discrete Kalman filter with application on benchmark problems," *Expert Systems with Applications*, vol. 200, p. 117065, 2022, https://doi.org/10.1016/j.eswa.2022.117065.

[48] S. Narayanasami et al., "An Enhanced Trust-Based Kalman Filter Route Optimization Technique for Wireless Sensor Networks," *Wireless Personal Communications*, vol. 127, no. 2, pp. 1311–1329, 2022, https://doi.org/10.1007/s11277-021-08578-x.

[49] C. F. Pană *et al*., "Fuzzy Control of the Robotic Arm for a Smart Electric Wheelchair to Assist People with Movement Disabilities," *2021 22nd International Carpathian Control Conference (ICCC)*, pp. 1-6, 2021, https://doi.org.10.1109/ICCC51557.2021.9454626.

[50] H. Nguyen Minh, H. Trinh An, G. Tran Thi Cam, L. Dinh Thi Ha, and H. Do Quoc, "Fuzzy Logic and Quadtree-Based Control for Mobile Robots in Dynamic Environments," *Intelligent Robotics and Applications*, pp. 429–445, 2025, https://doi.org/10.1007/978-981-96-0777-8_31.

[51] K. K. Borkar *et al*., "Path planning design for a wheeled robot: a generative artificial intelligence approach," *International Journal on Interactive Design and Manufacturing (IJIDeM)*, vol. 19, no. 2, pp. 1315–1326, 2025, https://doi.org/10.1007/s12008-023-01721-x.

[52] S. Cebollada, L. Payá, M. Flores, A. Peidró, and O. Reinoso, "A state-of-the-art review on mobile robotics tasks using artificial intelligence and visual data," *Expert Systems with Applications*, vol. 167, p. 114195, 2021, https://doi.org/10.1016/j.eswa.2020.114195.

[53] H. Singh, P. Yadav, V. Rishiwal, M. Yadav, S. Tanwar, and O. Singh, "Localization in WSN-Assisted IoT Networks Using Machine Learning Techniques for Smart Agriculture," *International Journal of Communication Systems*, vol. 38, no. 5, 2025, https://doi.org/10.1002/dac.6004.

[54] H. Choi, M. Fujimoto, T. Matsui, S. Misaki and K. Yasumoto, "Wi-CaL: WiFi Sensing and Machine Learning Based Device-Free Crowd Counting and Localization," in *IEEE Access*, vol. 10, pp. 24395-24410, 2022, https://roi.org/10.1109/ACCESS.2022.3155812.

[55] P. Roy and C. Chowdhury, "A Survey of Machine Learning Techniques for Indoor Localization and Navigation Systems," *Journal of Intelligent & Robotic Systems*, vol. 101, no. 63, 2021, https://doi.org/10.1007/s10846-021-01327-z.

[56] J. Saini, M. Dutta, and G. Marques, "Fuzzy Inference System Tree with Particle Swarm Optimization and Genetic Algorithm: A novel approach for PM10 forecasting," *Expert Systems with Applications*, vol. 183, p. 115376, 2021, https://doi.org/10.1016/j.eswa.2021.115376.

[57] R. K. Huda and H. Banka, "Efficient feature selection methods using PSO with fuzzy rough set as fitness function," *Soft Computing*, vol. 26, no. 5, pp. 2501–2521, 2022, https://doi.org/10.1007/s00500-021-06393-x.